Direct numerical simulation of dense particle-laden flows using a conservative immersed boundary technique

By P. Pepiot† AND O. Desjardins‡

Dense particle-laden flows are challenging to model because of their inherent multiphysics and multiscale nature. In order to improve our understanding of these flows and develop efficient simulation strategies, analysis from first-principles is warranted. This paper presents the development and validation of a direct numerical simulation approach where the flow around individual particles is fully resolved. Based on the recent conservative immersed boundary scheme of Meyer *et al.* (2010), the approach allows for the representation of a large number of moving and colliding objects without requiring a body-fitted grid. Fluid mass is conserved discretely, and momentum is exchanged conservatively between the fluid and the particles. This approach provides a second order accurate drag force on the particles. It is then validated by comparing the drag coefficient of isolated cylinders and spheres at various Reynolds numbers with theory. The effect of particle packing on drag is also considered, and good agreement is obtained with previous studies for both simple cubic and random particle arrangements. Finally, freely moving particles are simulated, showing a significant departure in drag force with the stationary case.

1. Introduction

Dense particle-laden turbulent flows are encountered in a vast number of engineering applications, ranging from pharmaceutical coatings to chemicals synthesis. Of particular interest to the National Renewable Energy Laboratory are the flows encountered in fluidized beds. Indeed, the thermochemical conversion of biomass to biofuels relies heavily on good mixing properties and homogeneous heating rates. However, dense particulate systems are especially challenging to model accurately because they involve multiple physical processes acting over a range of length scales. Micro-scales are dominated by boundary layers at the surface of the particles and inter-particle collisions, themselves controlled by complex contact mechanics. Inhomogeneities in the gas-solid system originate from particle clustering at the meso-scale, and gas bubbles at the macro-scale, for which the formation mechanism is still unclear.

There are two main modeling approaches suitable for the simulation of reactors. Eulerian methods are built on the assumption that the solid and gas phases are two interpenetrating media, and usually use the kinetic theory of gases to derive the governing equations (Gidaspow 1994). On the other hand, the Lagrangian particle tracking (LPT) technique uses a Monte-Carlo approach to solve the dispersed phase by considering each particle independently and solving for their trajectories (Deen *et al.* 2007). Resolving down to the particle scale is not affordable for problems of practical interest, which can

† National Renewable Energy Laboratory, Golden, CO, USA.
‡ Mechanical Engineering, University of Colorado at Boulder, Boulder, CO, USA.

involve billions of particles when considering industrial reactors. Therefore, the particle scales are usually filtered out, following for example the volumetric averaging procedure of Anderson & Jackson (1967) or the ensemble averaging procedure of Zhang & Prosperetti (1997). The filtering operation introduces an unclosed sub-filter stress tensor in the gas phase equations that needs to be modeled. These sub-filter stresses are often ignored, or at best crudely approximated. In addition, the drag force on the particles is no longer readily available, and needs to be modeled as well. Such drag models typically account for Reynolds number and particle packing effects, but they ignore other potential effects, such as particle acceleration, collisions, and sub-filter inhomogeneities in the flow field. Direct numerical simulation (DNS) is an elegant and accurate way to develop new models, but it presents significant numerical challenges, especially when considering non-stationary systems and high particle packing. In this context, immersed boundaries (IB) approaches can provide a appealing way to describe the gas particle interface.

In this work, the conservative IB formulation of Meyer *et al.* (2010) has been coupled to a Lagrangian particle tracking scheme to handle moving objects through the introduction of a level set function. The approach has been first validated on stationary systems such as isolated cylinders and spheres, and arrangements of spheres previously investigated using Lattice-Bolzmann simulations. A simulation of freely moving spheres falling under gravity is then presented to examine the effect of collisions and finite Stokes number on the drag forces acting on the particles.

2. Mathematical formulation

2.1. *Gas phase*

We assume the fluid to obey the low-Mach number Navier-Stokes equations. Because we are interested in solving the flow past resolved particles, the interaction between fluid and solid explicitly appears as a boundary condition. Conservation of mass is written as

$$\frac{\partial \rho}{\partial t} + \nabla \cdot (\rho \boldsymbol{u}) = 0, \tag{2.1}$$

where $\boldsymbol{u}$ is the fluid velocity, ρ is the fluid density, and t is time. Similarly, conservation of momentum is written as

$$\frac{\partial \rho \boldsymbol{u}}{\partial t} + \nabla \cdot (\rho \boldsymbol{u} \otimes \boldsymbol{u}) = \nabla \cdot \boldsymbol{\tau} + \rho \boldsymbol{g}, \tag{2.2}$$

where $\boldsymbol{g}$ is the gravitational acceleration and $\boldsymbol{\tau}$ is the stress tensor. The stress tensor is defined by

$$\boldsymbol{\tau} = -p\, \mathcal{I} + \boldsymbol{\sigma}, \tag{2.3}$$

where p is the pressure and $\boldsymbol{\sigma}$ is the viscous stress tensor, defined by

$$\boldsymbol{\sigma} = \mu \left(\nabla \boldsymbol{u} + \nabla \boldsymbol{u}^{\mathsf{T}} \right) - \frac{2}{3} \mu \nabla \cdot \boldsymbol{u}\, \mathcal{I}, \tag{2.4}$$

with μ the dynamic viscosity coefficient. Note that in this paper, the gas density and viscosity are kept constant. Finally, at the surface S_p of each particle p with velocity $\boldsymbol{u}_p$, we can write the no-slip and no-penetration conditions, i.e., $\boldsymbol{u}|_{S_p} = \boldsymbol{u}_p$.

2.2. *Particle phase*

We solve for the translational motion of the particles, neglecting the rotational motion. The position of an individual particle p evolves according to

$$\frac{d\boldsymbol{x}_p}{dt} = \boldsymbol{u}_p, \tag{2.5}$$

where $\boldsymbol{x}_p$ is the position of a particle and $\boldsymbol{u}_p$ is its velocity, which according to Newton's second law of motion obeys

$$m_p \frac{d\boldsymbol{u}_p}{dt} = \boldsymbol{f}_d + \boldsymbol{f}_c + m_p \boldsymbol{g}. \tag{2.6}$$

In the previous equation, m_p is the mass of the particle, defined by $m_p = \pi \rho_p d_p^3/6$ where ρ_p is the particle density and d_p is the particle diameter. $\boldsymbol{f}_c$ is the particle collision force, which is obtained from a soft-sphere collision model, details of which can be found for example in Deen *et al.* (2007). $\boldsymbol{f}_d$ is the drag force, which can be expressed as

$$\boldsymbol{f}_d = \int_{S_p} \boldsymbol{\tau} \cdot \boldsymbol{n} dS. \tag{2.7}$$

In the previous relation, $\boldsymbol{n}$ is the normal vector to the particle surface S_p.

3. Numerical approach

The equations presented above are implemented in the flow solver NGA (Desjardins *et al.* 2008), an arbitrarily high order multiphysics CFD code that uses mass, momentum, and kinetic energy conserving spatial discretizations. For all simulations presented below, the computations are performed using second order accuracy in space and time. Time advancement of the gas phase is accomplished using the semi-implicit Crank-Nicolson scheme of Pierce & Moin (2001), while the particles are advanced using a second order Runge-Kutta solver. Coupling between particles and gas is performed once between each time step.

For conciseness, the full details of the algorithm are not reported here. Instead, we will provide a brief summary of the computational approach employed. For the details of the implementation of the conservative immersed boundaries for stationary objects, the reader is referred to Meyer *et al.* (2010). The center of mass of each particles is updated using a Lagrangian particle tracking scheme. From the knowledge of the position and diameter of each particle, a signed distance function scalar ϕ is constructed to identify the particle surface explicitely, i.e.,

$$\phi(\boldsymbol{x}) = \min_{\text{all particles}} \left(|\boldsymbol{x} - \boldsymbol{x}_p| - \frac{d_p}{2} \right). \tag{3.1}$$

The IB algorithm requires the knowledge of the gas volume fraction, particle surface area, and face apertures for each cell in the computational domain. Whereas several strategies can be used to compute such quantities, we choose here to triangulate the gas-solid interface using a marching tetrahedra algorithm to identify the $\phi = 0$ iso-surface. This approach, while tedious to implement, has the advantage of being purely geometric and formally second order accurate. The volume fraction and face apertures can then be readily used to rescale the fluxes in NGA according to Meyer *et al.* (2010).

In addition, several interfacial fluxes need to be provided in all cut cells. For simplicity,

they are provided in the form of source terms in the Navier-Stokes equations, and include (a) the viscous effect on the particle surface

$$\int_{S_{p,k}} \boldsymbol{\sigma} \cdot \boldsymbol{n} dS \approx \int_{S_{p,k}} \mu \frac{d\boldsymbol{u}_t}{dn} dS \,, \tag{3.2}$$

where $S_{p,k}$ is the portion of the particle surface in the cell k, n is the curvilinear abscissa in the normal direction to the surface, and

$$\boldsymbol{u}_t = \boldsymbol{u} - (\boldsymbol{u} \cdot \boldsymbol{n})\, \boldsymbol{n} \,, \tag{3.3}$$

(b) the convective flux due to particle motion

$$\int_{S_{p,k}} \rho \boldsymbol{u} \otimes \boldsymbol{u} \cdot \boldsymbol{n} dS \,, \tag{3.4}$$

with its counterpart in the continuity equation

$$\int_{S_{p,k}} \rho \boldsymbol{u} \cdot \boldsymbol{n} dS \,. \tag{3.5}$$

At the particle surface, the gas velocity is equal to the particle velocity, hence these fluxes can readily be evaluated. Particle forces are finally created using Eq. 2.7, for which the viscous contribution can be obtained from Eq. 3.2, and the pressure contribution is obtained from an additional surface integration. The overall strategy has several benefits; fluid mass is discretely conserved. Momentum is exchanged in a conservative manner between the two phases because the flux terms that account for the presence of the particles in the fluid equations are directly used to create the force exerted by the fluid on the particle.

4. Stationary cylinders and spheres

4.1. *Flow past stationary, isolated cylinders and spheres*

The flow past a fixed cylinder is considered first. The two-dimensional computational domain is $20\, d_p \times 20\, d_p$. A uniform velocity U_∞ is imposed on the left boundary. A convective outflow boundary condition is imposed at the exit, and periodic conditions are imposed on all other sides of the domain. The Reynolds number, defined as $\mathrm{Re} = \rho d_p U_\infty / \mu$ is varied by changing the fluid viscosity.

A grid refinement study is conducted to assess the convergence properties of the numerical approach. The Reynolds number is set to 10, which is typical of what is encountered in fluidized bed reactors. Four configurations are simulated with 6.4, 12.8, 25.6, and 51.2 grid points per diameter, respectively. The finest grid serves as the reference case. The error on the drag coefficient $C_D = |\boldsymbol{f}_d| / \left(\frac{1}{2}\rho U_\infty^2 L_z d_p\right)$ is reported in Fig. 1. A convergence between second and third order is obtained. Even with 6 grid points per diameter, an error of less than 10% is observed, indicating that this approach will allow one to reach large numbers of particles at a limited computational cost.

Figure 2(a) shows the evolution of the drag coefficient C_D as function of the Reynolds number. The standard drag curve is compared with the simulation results obtained using 12.8 grid points per diameter. The computational domain is the same as described above. A good agreement is obtained over the range of Reynolds numbers considered in the study. The drag force is slightly over-estimated at very low Reynolds number, which can be explained by the increasing role of confinement when viscous effects become dominant.

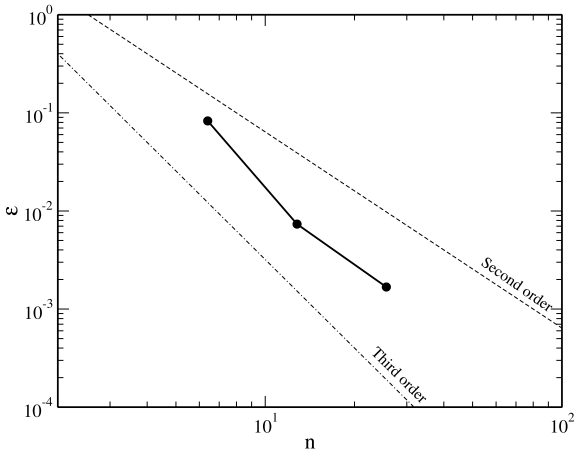

FIGURE 1. Error ε in the prediction of the drag coefficient C_D as function of the number of grid points per diameter n for a stationary cylinder at $\mathrm{Re} = 10$.

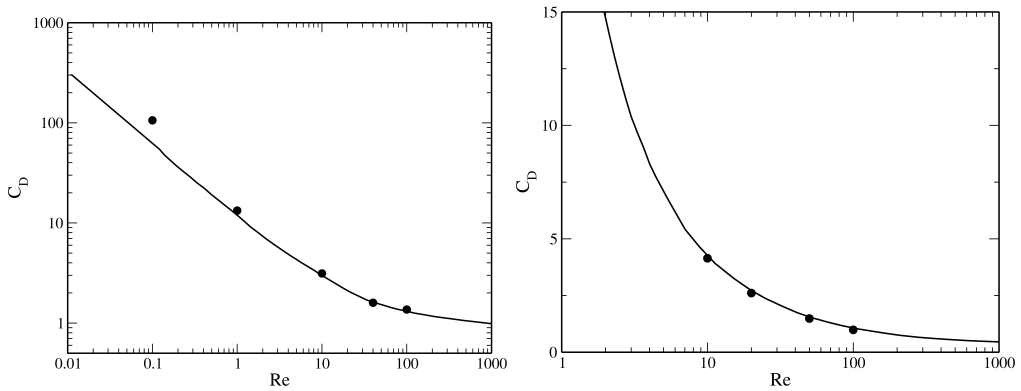

(a) Cylinder. (b) Sphere.

FIGURE 2. Drag coefficient C_D for flows over a stationary object at various Reynolds numbers: Simulations (symbols) and standard drag coefficient curves (line; Clift *et al.* 1978).

At $\mathrm{Re} = 100$, the Strouhal number $\mathrm{St} = f d_p/U_\infty$, where f is the frequency of the vortex shedding behind the cylinder, is 0.173 when based on the oscillation of the drag coefficient. This result is in agreement with the experimental value of 0.165 reported by Williamson (1992).

A similar study is conducted for flows past a stationary sphere. The computational domain is now $20\,d_p \times 20\,d_p \times 20\,d_p$, and the sphere is represented using 12.8 grid points in the diameter. Results for the drag coefficient are shown in Fig. 2(b) and are in very good agreement with the experimental curve (Clift *et al.* 1978).

4.2. *Flow past sphere arrays*

The next step in our validation study is to consider periodic arrangements of spheres. In this case, as mentioned by Beetstra *et al.* (2007), the non-negligible volume of the spheres, along with the forcing used to drive the gas flow, introduces some ambiguity in the way the Reynolds number and drag force are defined. Therefore, we will start by carefully defining several quantities of interest.

The average fluid flow velocity $\boldsymbol{u}_0$ is defined as

$$\boldsymbol{u}_0 = \frac{1}{V_f}\int_{V_f} \boldsymbol{u}\, dV\,, \tag{4.1}$$

where V_f is the total volume occupied by the gas. The superficial velocity $\boldsymbol{U}_0$ corresponds to the velocity of the gas were the spheres to be removed, and is related to $\boldsymbol{u}_0$ by $\boldsymbol{U}_0 = \varepsilon \boldsymbol{u}_0$, with ε being the average gas volume fraction in the computational domain. In the following, the particle Reynolds number will be based on the superficial velocity $\boldsymbol{U}_0$

$$\mathrm{Re} = \frac{\rho d_p |\boldsymbol{U_0}|}{\mu}\,. \tag{4.2}$$

The flow past a periodic static array of spheres is maintained using a body force, which may take the form of a mean pressure gradient. Because computing the particle drag involves integrating the pressure over the surface of the particle, using such a forcing pressure gradient will lead to a total force on the particle $\boldsymbol{f}_t$ that includes both the drag force $\boldsymbol{f}_d$ and the effect of the mean pressure gradient ∇P. A simple balance of forces yields $\boldsymbol{f}_d = \varepsilon \boldsymbol{f}_t$ (Beetstra *et al.* 2007). The results reported here are shown in terms of the drag force $\boldsymbol{f}_d$, non-dimensionalized by the Stokes drag based on the superficial velocity $\boldsymbol{U}_0$

$$F = \frac{|\boldsymbol{f}_d|}{3\pi\mu d_p |\boldsymbol{U}_0|}\,. \tag{4.3}$$

The dimensionless drag force is usually assumed to be a function of the Reynolds number and local gas volume fraction. Note that if the particle is moving, the previous definitions still apply, provided we switch to the frame of reference attached to the particle.

4.2.1. *Simple cubic arrangement*

To investigate the effect of packing on the drag force, simple cubic arrangements of spheres are first considered. The configurations are chosen following the work of Hill *et al.* (2001), who used Lattice-Boltzmann (LB) simulations to compute the drag exerted on periodic arrays of spheres. In each case, the computational domain is a cubic box containing a single sphere. Periodic boundary conditions are imposed on all six faces. The dimensions of the box are chosen so that the different packing values used by Hill *et al.* (2001) are recovered. A uniform gas velocity is imposed initially, and a body force term in the Navier-Stokes equations enforced that the integral of the velocity over the gas phase domain remains constant throughout the simulation. Note that in the work by Hill *et al.* (2001), both the Reynolds number and the drag force definitions differ from the present work, and their results have been transformed accordingly. A comparison of the obtained dimensionless drag force is shown in Fig. 3. A good agreement is observed between both simulation results, even if LB values are generally higher. However, they were obtained using a coarse lattice, and grid refinement was shown to lead to lower drag forces, which is consistent with our results.

4.2.2. *Uniform random arrangement*

The next step considers random arrangements of spheres. Spheres are randomly generated inside a cubic domain of dimension $(14d_p)^3$ according to a uniform distribution. A few relaxation steps done prior to the start of the simulations permit the removal of any initial overlap between the spheres. To speed up statistical convergence, a relatively large number of spheres is used, and each condition is simulated twice. The configuration

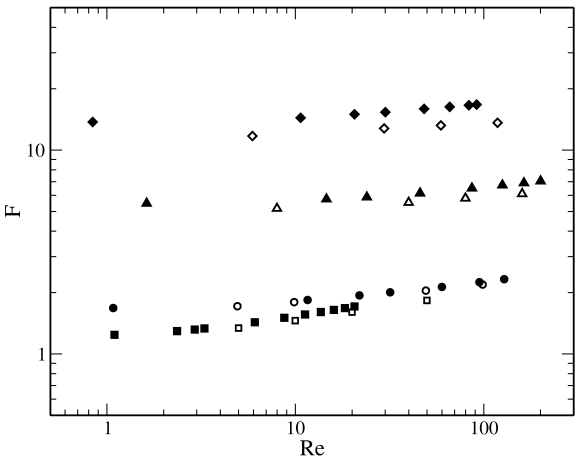

FIGURE 3. Non-dimensional drag force as function of the particle Reynolds number for simple cubic arrangements of spheres. Comparison between Hill *et al.* (2001) (filled symbols) and present work (open symbols). $\varepsilon = 0.999$ (squares), 0.9859 (circles), 0.799 (triangles), and 0.594 (diamonds).

matrix includes three packing values and three different Reynolds numbers, with the number of spheres varying between 500 and 1500. The spheres are represented with 12.8 grid points per diameter.

Lattice-Boltzmann simulations of flows past random arrays of spheres have been used by Beetstra *et al.* (2007) to derive correlations for the dependence of F in terms of gas volume fraction and particle Reynolds number. They proposed the following model for F that is applicable to a wide range of Reynolds numbers and gas volume fractions.

$$\begin{aligned} F(\varepsilon, \mathrm{Re}) =& 10\frac{1-\varepsilon}{\varepsilon^2} + \varepsilon^2\left(1 + 1.5\sqrt{1-\varepsilon}\right) \\ &+ \frac{0.413\mathrm{Re}}{24\varepsilon^2}\left(\frac{\varepsilon^{-1} + 3\varepsilon(1-\varepsilon) + 8.4\mathrm{Re}^{-0.343}}{1 + 10^{3(1-\varepsilon)}\mathrm{Re}^{-0.5-2(1-\varepsilon)}}\right). \end{aligned} \tag{4.4}$$

The dimensionless drag force obtained using the immersed boundary approach is compared to Eq. 4.4 in Fig. 4. The IB simulations match Beetstra's model fairly well for Reynolds numbers below 10. However, they depart significantly at higher Re. This was observed before with a different immersed boundary approach by Subramanian *et al.* (2010) and attributed to the forcing technique used in the LB simulations. Less than 2% scatter is observed across the different replicates of each configuration, indicating that the number of spheres is large enough to obtain statistical convergence. It would be of interest to simulate similar flows using more complex random distributions instead of the uniform distribution considered here. However, this falls outside of the scope of the present work.

5. Freely falling spheres

Finally, the effect of particle motion on the drag force is investigated. The computational domain is set to $(15d_p)^3$, and the gas volume fraction is 0.8, leading to a total of 1330 spheres. Periodic conditions are imposed on all sides. The spheres are initially arranged in arrays, and a small random particle velocity is imposed to accelerate flow

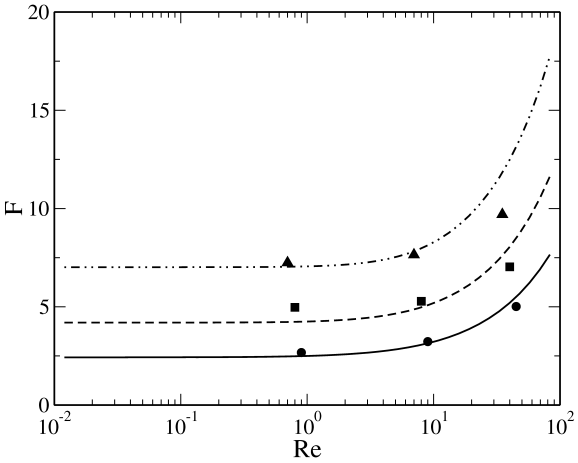

FIGURE 4. Non-dimensional drag force as function of the particle Reynolds number for random arrangements of spheres. Comparison between the model of Beetstra *et al.* (2007) (lines) and present work (symbols). $\varepsilon = 0.9$ (circles), 0.8 (squares), and 0.7 (triangles).

destabilization. The spheres accelerate under gravity, whereas the mean gas velocity is maintained at zero through a body-forcing term.

The forces are analyzed at a single time after a statistically stationary state is reached. To analyze local packing and Reynolds number effects, and reproduce the conditions for which drag models such as the one shown in Eq. 4.4 are applicable, we introduce a volume filtering procedure (Anderson & Jackson 1967) and define local mean gas phase quantities. Filtered gas velocity and gas volume fraction are computed for each particle using a box filter centered on that particle. Three filter sizes are used, $15d_p$ (i.e., the full computational domain), $7.5d_p$, and $3.75d_p$.

The first quantity of interest is the mean drag force averaged over all particles, which can be compared to Beetstra's model using the mean Reynolds number and mean gas-volume fraction extracted from the moving particles simulation, and more interestingly, to the value obtained from the random stationary simulations. A good agreement with the latter would indicate that stationary systems are indeed a good representation of the moving particles configuration, and that particle acceleration and collisions play a minor role in the determination of the drag force. The comparison is shown in Fig. 5. Although remaining close, the drag force obtained in the case of moving particles shows some departure from the static results, therefore confirming that particle acceleration and collisions can affect the drag forces experienced by the particles. Figure 5 also shows a scatter plot of the drag force on individual particles, reported as a function of their individual Reynolds number. Clearly, the direction of the scatter is not aligned with Beetstra's model, which predicts that drag increases with the Reynolds number. This suggests that additional parameters that directly impact the drag force are not accounted for in the models. These results are obtained with the larger filter, although no significant differences are observed when using the smaller filter sizes.

Finally, a scatter plot relating the filtered gas volume fraction to the filtered Reynolds number for all three filter sizes is shown in Fig. 6. When the filter size corresponds to the domain size, the filtered gas volume fraction is equal to the mean value, whereas the Reynolds number, a strong function of the particle velocity, varies significantly. As the filter size is decreased, the spread in the filtered gas volume fraction increases. However,

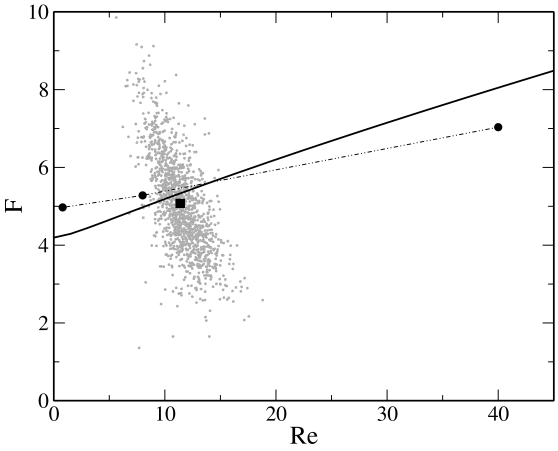

FIGURE 5. Dimensionless drag force as function of the particle Reynolds number with an overall gas volume fraction of 0.8. Comparison between the Beetstra *et al.* (2007) model (line), a stationary random arrangements of spheres (filled circles, dashed line), and moving spheres (average value (square) and scatter plot of forces on individual particles (grey dots) obtained using a filter size $\Delta = 15d_p$.)

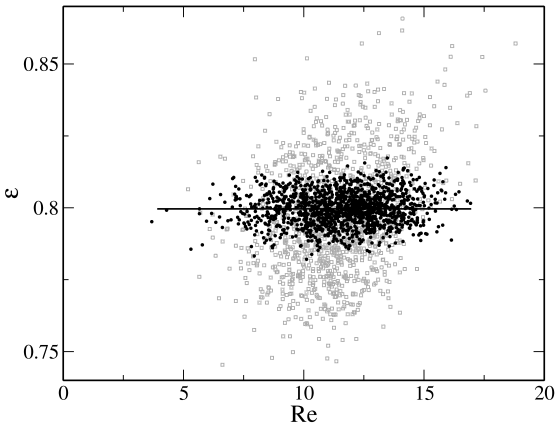

FIGURE 6. Scatter plot of the gas volume fraction and Reynolds number experienced by free–falling spheres for different filter sizes: $\Delta = 15d_p$ (line), $7.5d_p$ (black dots), and $3.75d_p$ (grey squares).

it is interesting to note that the filtered volume fraction and particle Reynolds number do not appear to be correlated, meaning that the departure from Beetstra's model observed in Fig. 5 cannot simply be explained by a local packing effect.

In summary, these results indicate that finite Stokes effects, collisions and sub-filter gradients may play an important role in the drag force of a moving particle in a dense gas-solid flow. This warrants further investigation in order to better understand what parameters govern particle drag.

6. Conclusions

A conservative immersed boundary scheme has been coupled with a Lagrangian particle tracking module within the flow solver NGA to provide a general framework for

the direct numerical simulation of complex gas-solid systems. The method has been used to investigate dense particle-laden flows in both stationary and non-stationary configurations. The approach has been validated with static flows and shows good agreement with prior work in the domain. More importantly, it was shown that drag forces experienced by moving particles can depart from stationary cases, on which most existing drag models are based. Further investigation is required to identify and quantify the causes of these discrepancies. The numerical tool developed as part of this study paves the way towards understanding the role played by particle acceleration and collisions as well as by sub-filter variations in velocity and gas volume fraction.

REFERENCES

Anderson, T. & Jackson, R. 1967 Fluid mechanical description of fluidized beds. equations of motion. *Ind. & Eng. Chem.* **6**, 527–529.

Beetstra, R., van der Hoef, M. A. & Kuipers, J. A. M. 2007 Drag force of intermediate reynolds number flow past mono- and bidisperse arrays of spheres. *AIChE J.* **53** (2), 489–501.

Clift, R., Grace, J. R. & Weber, M. E. 1978 *Bubbles, Drops, and Particles*. Academic Press, New York.

Deen, N. G., Van Sint Annaland, M., Van Der Hoef, M. A. & Kuipers, J. A. M. 2007 Review of discrete particle modeling of fluidized beds. *Chem. Eng. Sci.* **62**, 28–44.

Desjardins, O., Blanquart, G., Balarac, G. & Pitsch, H. 2008 High order conservative finite difference scheme for variable density low Mach number turbulent flows. *J. Comp. Phys.* **227** (15), 7125–7159.

Gidaspow, D. 1994 *Multiphase flow and fluidization: continuum and kinetic theory descriptions*. Academic press.

Hill, R. J., Koch, D. L. & Ladd, A. J. C. 2001 Moderate-reynolds-number flows in ordered and random arrays of spheres. *J. Fluid Mech.* **448**, 243–278.

Meyer, M., Devesa, A., Hickel, S., Hu, X. Y. & Adams, N. A. 2010 A conservative immersed interface method for large-eddy simulation of incompressible flows. *J. Comp. Phys.* **229**, 6300–6317.

Pierce, C. D. & Moin, P. 2001 Progress-variable approach for large eddy simulation of turbulent combustion. *Tech. Rep.* TF80. Flow Physics and Computation Division, Dept. Mech. Eng., Stanford University.

Subramanian, S., Tenneti, S., Garg, R., Devendran, K., Mehrabadi, M., Fox, R. O., Sundaresan, S. & Hrenya, C. M. 2010 Interaction of particles with carrier gas revealed by particle-resolved direct numerical simulation: Improved drag laws and models, NETL workshop on multiphase flows, Pittsburgh.

Williamson, C. H. K. 1992 The natural and forced formation of spot-like vortex dislocations in the transition of a wake. *J. Fluid Mech.* **243**, 393–441.

Zhang, D. Z. & Prosperetti, A. 1997 Momentum and energy equations for disperse two-phase flows and their closure for dilute suspensions. *Int. J. Multiphase flows* **23**, 425–453.